European Journal of Chemistry 4 (4) (2013) 425-433

European Journal of Chemistry

Journal homepage: www.eurjchem.com

Lead uptake by new silica-carbon nanoparticles

Hassan Hasan Hammud [a,*], Mayssam Mostafa Chahine [a], Bassem El Hamaoui [a] and Younes Hanifehpour [b]

[a] *Department of Chemistry, Faculty of Sciences, Beirut Arab University, Debbieh, 11-5020, Lebanon*
[b] *Nanoresearch Center, School of Mechanical Engineering, Yeungnam University, Gyongsan, 712-749, South Korea*

**Corresponding author at: Department of Chemistry, Faculty of Sciences, Beirut Arab University, Debbieh, 11-5020, Lebanon. Tel.: +961.3.381862; fax: +961.1.300110. E-mail address: h.hammud@bau.edu.lb (H.H. Hammud).*

ARTICLE INFORMATION

Received: 19 March 2013
Received in revised form: 09 June 2013
Accepted: 03 July 2013
Online: 31 December 2013

KEYWORDS

Lead
Kinetics
Adsorption
Thermodynamics
Silica-carbon nanoparticle
Scanning electron microscope

ABSTRACT

Silica-carbon nanoparticles (SCNP) were prepared from sonication of silica and anthracene. The size of homogenous nanoparticle is around 5-20 nm confirmed by Scanning Electron Microscopy (SEM) and Transmission Electron Microscopy (TEM). SEM analysis indicated surface porosity. SCNP were used to remove lead ions (Pb(II)) from aqueous solutions. Adsorption isotherm of Pb(II) on SCNP was well fitted in terms of the Freundlich and Langmuir models. The maximum adsorption capacity of SCNP for Pb(II) was found to be 385 mg/g (1.86 mmol/g) in batch experiment. Thermodynamic studies indicated that sorption process of lead onto SCNP was spontaneous and exothermic. A pseudo-second order model has been employed in order to describe the kinetic adsorption processes, and the thermodynamic activation parameters were calculated. In a column studies, q_y the Yan adsorption capacity of SCNP for Pb(II) was found to be 130.66 mg/g (0.63 mmol/g).

1. Introduction

Silica-Carbon nanoparticles (SCNP) can be defined as artificially composed structures with nanometer size (1.2-1.4 nm). Nowadays, they have a very wide range of possible applications making them valuable in electrical cables and wires [1], solar cells, ultra-capacitors, medical usage (e.g.: can be inserted around cancerous cells, then excited with radio waves, which causes them to heat up and kill the surrounding cells), etc. [2].

Although various methods of carbon nanoparticles production were developed since 1991, such as arc discharge [3], laser ablation [4], chemical vapor deposition [5] and solar technique [6], but their synthesis under ambient conditions, without defects, and with a high yield percentage remains a great challenge.

An innovative sonochemical method was introduced for high purity SCNP production at atmospheric pressure and room temperature [7]. It consists of bubbles cavitation produced in liquid solution during sonication. Local spots of several thousand degrees Celsius of temperature and several thousand atmospheres of pressure generated were able to produce SCNP and needs neither specialized equipment nor a multistep purification process [8].

Heavy metal ions in water have been a major preoccupation for many years because of their toxicity toward aquatic-life, plants, animals, human beings and the environment. As they do not degrade biologically like some organic pollutants, their presence in water is a public health problem due to their absorption and therefore possible accumulation in organisms [9]. Water contaminated by heavy metal ions had become much more serious with a rapid development of industries and competitive use of fresh water in many parts of the world. Therefore, heavy metal ions removal from water has become an important issue today [10].

Having a relatively large surface area, SCNP have attracted researchers' interest as a new type of adsorbent and offer an attractive option for the removal of organic and inorganic contaminants from water such as Pb(II) [11], Cd(II) [12], and Cr(III) [13]. In the present work, treatment of lead containing aqueous solution by adsorption technique is addressed. Equilibrium data, commonly known as adsorption isotherms, are the basic requirements for the design of adsorption systems.

2. Experimental

2.1. Silica-carbon nanoparticles preparation

The typical process of this method for SCNP growth is presented in Figure 1. The strategy begins by preparing a solution of anthracene in toluene. Silica powder and ferrocene were then added to this solution [14]. Ferrocene was chosen as a precursor of iron catalyst for nanotube growth. The carbon source for SCNP growth was provided by toluene, anthracene, as well as by ferrocene, while silica powder acted as a nucleation site. Ultrasonication was performed under ambient conditions with a power of 200 W for 2 hours. Finally, the resulting powder was collected on filter membrane. The products were characterized by field emission scanning electron microscopy, and thermal analysis.

2.2. Equipment and instrument

Thermogravimetric-differential thermal analysis (TG-DTA) curves were recorded from 20-700 °C on SETARAM LABSYS thermal analyzer in the flow of N_2 with a heating rate of 3

ISSN 2153-2249 (Print) / ISSN 2153-2257 (Online)
DOI:10.5155/eurjchem.4.4.425-433.776

°C/min. An ultrasonic homogenizer (Bandelin Sonopuls HD 2200) connected to an HF-generator 230 V and 50 Hz frequency was used for the ultrasonication and preparation of SCNP. A shaking incubator (SHIN SAENG SKIR-601 Model) was used for the shaking experiment, while water bath was used for standing experiment. Atomic absorption spectrophotometer (Buck Scientific) was used in order to determine the concentration of Lead in solution. The morphology of the materials was examined using a JEOL JSM6700F Scanning Electron Microscope. Elemental analyses were carried out using a linked ISIS300, Oxford. The samples were coated with gold powder before SEM (Scanning Electron Microscopy) and EDX (energy dispersive X-Ray) measurements. The SAED pattern was recorded by a Cs-corrected high-resolution TEM (JEM-2200FS, JEOL) operated at 200 kV.

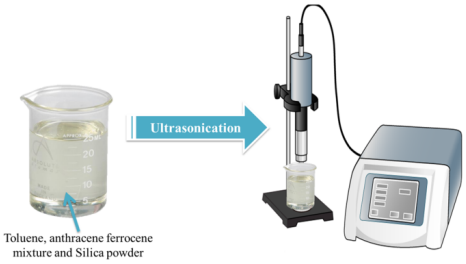

Figure 1. Typical process for SCNP growth by ultrasonication.

2.3. Preparation of lead solution

Lead stock solution was prepared by dissolving 1.5984 g of lead nitrate $Pb(NO_3)_2$ in 500 mL of distilled water. The stock solution was used to prepare 100, 200, 300, 400, 500 and 600 mg/L solutions.

2.4. Batch experiments

A series of batch experiments were conducted to explore the effect of various factors such as the contact time, shaking, the initial concentration of adsorbate and temperature on the adsorption process.

2.4.1. Standing experiments

Batch adsorption experiments were conducted in 50 mL volumetric flasks in a water bath, by taking a specified amount (0.05 g) of adsorbent with 50 mL of lead solution of specified concentration. The mixture was left to stand with no shaking.

2.4.2. Shaking experiments

Batch adsorption experiments were conducted in 100 mL volumetric flasks by taking a specified amount (0.05 g) of adsorbent with 50 mL of lead solution of specified concentration. The contents of the flasks were shaken at 160 rpm on the Shaker Incubator at fixed temperature. At different time, the concentration of lead remaining in solution was determined through transferring the extracted sample (1 mL) to an Erlenmeyer flask diluted, then analyzed for Pb(II).

The adsorption capacity of SCNP was determined by material balance of the initial and equilibrium concentrations of the solution. The amount adsorbed per unit mass of adsorbent at equilibrium was obtained from the relationship in Equation (1) [15].

$$Q_e = \frac{(C_0 - C_e)V}{m} \quad (1)$$

where, Q_e (mg/g) is the adsorption capacity at equilibrium, C_0 and Ce denote the initial and equilibrium concentrations of the lead solutions in (mg/L), V is volume of the solution in mL and m is the mass of the adsorbent used in gram [16].

3. Theory

3.1. Kinetics

3.1.1. Pseudo-first-order kinetic model

This model assumes that the rate of change of the solute uptake with time is directly proportional to the difference in saturation concentration and the amount of solid uptake with time [17,18].

The rate constant of adsorption is expressed as a pseudo-first-order rate expression given as in Equation (2) [19].

$$\frac{dq}{dt} = K_1(q_e - q_t) \quad (2)$$

where, q_e and q_t are the amount of lead adsorbed (mg/g) at equilibrium and at contact time t (min) respectively, K_1 is the pseudo-first-order rate constant (min^{-1}).

Integrating with the boundary conditions at $t = 0$, $q_t = 0$ and at $t = t$, $q = q_t$ and rearranging Equation (2), the rate law for a pseudo-first-order reaction becomes Equation (3).

$$\text{Log}\,(q_e\text{-}q_t) = \text{Log}\,q_e - \frac{K_1}{2.3}t \quad (3)$$

When adsorption is preceded by diffusion through a boundary, the kinetics in most cases follow the pseudo-first-order rate equation of Lagergren $K_1(q_e\text{-}\ q_t)$ represent the number of available sites [20].

3.1.2. Pseudo-second-order kinetic model

The sorption kinetics may be represented by pseudo-second-order model as in Equation (4).

$$\frac{dq}{dt} = K_{II}(q_e - q)^2 \quad (4)$$

where, K_{II} is the equilibrium rate constant for pseudo-second-order sorption (g/mg.min). Integrating Equation (4) using the boundary conditions at t = 0, $q_t = 0$ and at $t = t$, $q = q_t$ and rearranging Equation (4), the rate law for a pseudo-second-order reaction becomes Equation (5) [21].

$$\frac{t}{q_t} = \frac{1}{K_{II} \times q_e^2} + \frac{t}{q_e} \quad (5)$$

If the pseudo-second-order kinetic is applicable, the plot gives a linear relationship which allows computation of K_{II} and q_t.

3.1.3. Intra-particle-diffusion model

In general, the lead sorption is governed by either the liquid phase mass transport rate or through the intra-particle mass transport rate. Thus, the adsorption process is a diffusive mass transfer process where the rate can be expressed in terms of the square root of time $t^{1/2}$. The mathematical dependence of q_t versus $t^{1/2}$ is obtained if the process is considered to be influenced by diffusion in the particles and convective diffusion in the solution. According to the intra-particle diffusion model proposed by Weber and Morris [22], the root time dependence may be expressed by Equation (6).

$$q_t = K_i\sqrt{t} + I \quad (6)$$

where, q_t is the fraction lead uptake (mg/g) at time t, K_i is the intra-particle diffusion rate constant (mg.g^{-1}.min$^{-1/2}$) and I is the intercept (mg/g).

If the intra-particle diffusion is involved in the adsorption process, then the plot of the square root of time versus the uptake would result in a linear relationship. The plot will give K_i as slope and I as intercept. The minimum the intercept length, the adsorption is less controlled by boundary layer. In this case, the intra-particle diffusion would be the controlling step if this line passed through the origin. When the plots do not pass through the origin, this is indicative of some degree of boundary layer control and this further show that the intra-particle diffusion is not the only rate controlling step, but also other processes may control the rate of adsorption.

3.2. Adsorption isotherm

Adsorption properties and equilibrium data, commonly known as adsorption isotherms, describe how pollutants interact with sorbent materials and so are critical in optimizing the use of adsorbents. There are several isotherm equations available for analyzing experimental sorption equilibrium data, including Freundlich, Langmuir, Toth, Temkin, Elovich, Redlich-Peterson, Sips and Dubinin-Radushkevich isotherms. However, the two most common types of isotherms are Freundlich and Langmuir models, and Langmuir sorption isotherm is the best known of all isotherms describing sorption [23,24].

In the present work, equilibrium studies were carried out at different temperatures (25, 30, 35 and 40 °C). The equilibrium data were analyzed using: Langmuir, Freundlich, Temkin, and Elovich isotherms models.

3.2.1. Langmuir model

The Langmuir isotherm considers sorption as a chemical phenomenon [25]. Langmuir's isotherm is known as monolayer adsorption onto a surface with a finite number of similar active sites.

The well-known non-linear and linear expressions of the Langmuir model are given by Equations (7) and (8), respectively [25].

$$Q_e = \frac{Q^0 K_L C_e}{1 + K_L C_e} \tag{7}$$

$$\frac{1}{Q_e} = \frac{1}{Q^0 K_L}\frac{1}{C_e} + \frac{1}{Q^0} \tag{8}$$

where Q^0 and K_L are the parameters, Q^0 (mg/g) is the maximum sorbate uptake under the given conditions. K_L is a coefficient related to the affinity between the sorbent and sorbate [26].

The essential characteristics of Langmuir isotherm can be expressed in terms of a dimensionless constant separation factor R_L which is defined by Equation (9) [27].

$$R_L = \frac{1}{1 + K_L C_o} \tag{9}$$

where, C_o is the highest initial lead concentration. For a favorable adsorption R_L value must be between 0 and 1. If R_L = 0 adsorption is irreversible, R_L = 1 adsorption is linear and for R_L >1 adsorption is unfavorable [28].

3.2.2. Freundlich model

The Freundlich isotherm is the earliest known relationship describing the sorption equation [29]. The model applies to adsorption on heterogeneous surfaces with interaction between adsorbed molecules and the application of the Freundlich equation also suggests that sorption energy exponentially decreases on completion of the sorption centers of an adsorbent [30].

The Freundlich relationship is exponential, Equation (10).

$$Q_e = K_F (C_e)^{1/n} \tag{10}$$

The linear form of the Freundlich equation Equation (11) employed to describe heterogeneous systems was used to find the adsorption isotherm.

$$\text{Ln } Q_e = \text{Ln } K_F + \frac{1}{n} \text{Ln } C_e \tag{11}$$

where, K_F and n are Freundlich constants. The Freundlich isotherm constant $n_F = (1/n)$, indicates the heterogeneity factor, n_F values lower than 1 interpret the strong adsorption between adsorbent and sorbate.

3.2.3. Temkin model

Temkin model explains sorbent/sorbate interactions in relation to heat of adsorption [15]. Non-linear and linear Temkin Equation (12) and (13) are:

$$Q_e = \frac{RT}{b} \text{Ln } (K_T C_e) \tag{12}$$

$$Q_e = B_T \text{Ln } (K_T) + B_T \text{Ln } (C_e) \tag{13}$$

where $B_T = (RT/b)$ is a factor related to the heat of adsorption and K_T is Temkin equilibrium constant (L/mg).

3.2.4. Elovich model

Elovich models deals with multilayer adsorption, based on a kinetic principle that adsorption site increase exponentially with adsorption. K_E is Elovich equilibrium constant and Q_E is Elovich maximum adsorption capacity [15]. Non-linear and linear Elovich forms are described in Equation (14) and (15).

$$\frac{Q_e}{Q_E} = K_E C_e \exp(-\frac{Q_e}{Q_E}) \tag{14}$$

$$\text{Ln } (\frac{Q_e}{C_e}) = \text{Ln } (K_E Q_E) - \frac{Q_e}{Q_E} \tag{15}$$

3.3. Sorption in a fixed bed column

Column study is a method used to develop a suitable regeneration method to reuse SCNP for multi-operational cycles.

3.3.1. Thomas kinetic model

Thomas model is a kinetic model used to analyze the column performance. It has been used by many researchers to study packed bed adsorption kinetics [31]. The linearized form of the Thomas model is described by Equation (16) [32].

$$\text{Ln } (\frac{C_0}{C_e} - 1) = \frac{K_T q_0 M}{Q} - \frac{K_T C_0}{Q} V \tag{16}$$

Where Ce and Co are the effluent and inlet solute concentrations (mg/L), q_o = the maximum adsorption capacity (mg/g), M = the total mass of the adsorbent (g), Q = volumetric flow rate (mL/min), V = the throughput volume (mL) and K_T = the Thomas rate constant (mL.min^{-1}.mg^{-1}). The kinetic

coefficient, K_T and the adsorption capacity of the bed, q_o were determined from the plot of Ln[(C_o/C_e)-1] against V at a given flow rate.

3.3.2. Yoon and Nelson kinetic model

Another kinetic model used in the study of column adsorption kinetics is Yoon and Nelson model [33]. The linear form of Yoon and Nelson model is represented in Equation (17).

$$\mathrm{Ln}\left(\frac{C_e}{C_0-C_e}\right)=K_{YN}t-\tau K_{YN} \quad (17)$$

where, K_{YN} is Yoon and Nelson rate constant, C_e and C_o are the effluent and inlet solute concentrations, τ is the time required for 50% adsorbate breakthrough (min) and t is the breakthrough (sampling) time (min). A plot of ln $C_e/(C_o-C_e)$ versus t gives a straight line with slope of K_{YN}, and intercept of $-\tau.K_{YN}$.

3.3.3. Yan et al. kinetic model

Yan *et al*. proposed an empirical equation which could overcome the draw-back in Thomas model especially its serious deficiency in predicting the effluent concentration with respect to time zero. The empirical equation proposed by Yan *et al*. was found a better description of the breakthrough curves in a fixed bed column. This equation is expressed as follows [34].

$$\mathrm{Ln}\left(\frac{C_e}{C_0-C_e}\right)=\frac{K_yC_0}{Q}\ \mathrm{Ln}\left(\frac{Q^2}{K_yq_ym}\right)+\frac{K_yC_0}{Q}\mathrm{Ln}\ t \quad (18)$$

where K_y is the kinetic rate constant for Yan Model (L.min^{-1}.mg^{-1}); q_y is the maximum adsorption capacity (mg/g) of adsorbent estimated by Yan Model.

3.3.4. Q_{max} calculation

The area under the breakthrough curve shows the total adsorbed pollutant quantity or the total mass of metal biosorbed (q_{total}), in mg, in the column for a given feed concentration and flow rate, and it can be calculated by the following integration [31].

$$q_{total}=\frac{Q}{1000}\int_{t=0}^{t=t_{total}}C_{ads}dt=\frac{QA}{1000} \quad (19)$$

where t and Q are the total flow rate (min) and volumetric flow rate (mL/min), respectively. Integrating the adsorbed concentration (C_{ad}; mg/L) versus t (min) plot showed the area under the breakthrough curve (A). The maximum capacity of the column (q_{max}) can be calculated q_{max} (mg/g) = q_{total} / m, where m is the sorbent mass (g).

4. Results and discussions

4.1. Characterization of silica-carbon nanoparticles

4.1.1. Thermal analysis data and discussion

The thermal analysis study of Silica-Carbon nanoparticles were done under N_2 by heating from 20 to 700 °C, Figure 2. The TGA (Thermo gravimetric analysis) curve indicated a sharp mass loss (7.0 %) in the temperature range 25 to 200 °C due to loss of hydroxyl group from silica and crystalline organic solvent; and a gradual mass loss (5.0 %) in the range 200-700 °C due to decomposition of SCNP materials. The DTA (Differential thermal analysis) curve indicated an exothermic process (peak) occurring at 290 °C with an associated enthalpy = -11.00 J/g. The exothermic process indicated extra carbon-carbon bonds formation in SCNP materials [24].

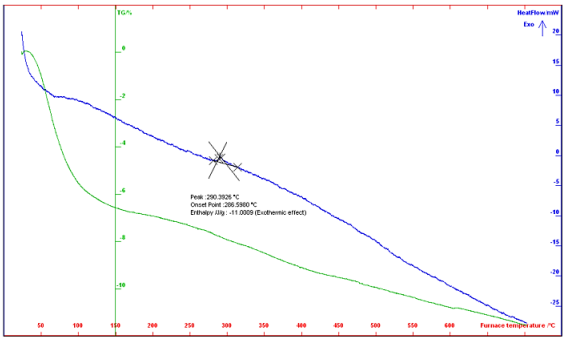

Figure 2. TGA and DTA curves of SCNP heated from 20 to 700 °C under N_2.

4.1.2. SEM discussion and figures

The nanoparticle size is around 5-20 nm confirmed by Transmission Electron Microscopic analysis (TEM). The Scanning Electron Microscopic analysis (SEM) indicated surface porosity (Figure 3), which may increase the adsorption capacity of heavy metals present in water. Diffraction pattern also show that samples are homogeneous nanoparticle. Energy Dispersive X-Ray analysis confirmed the presence of carbon along with silica materials (Figure 4).

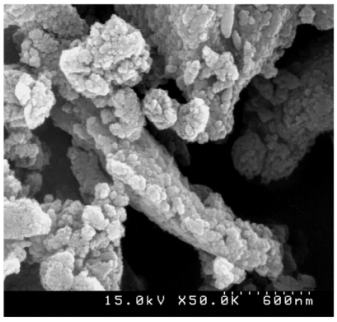

Figure 3. Scanning electron microscopy image of SCNP.

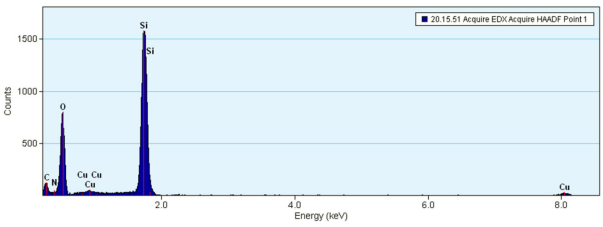

Figure 4. Energy Dispersive X-ray pattern of SCNP.

4.2. Effect of agitation speed

Agitation in a Shaker Incubator is an important parameter in adsorption phenomena, influencing the distribution of the solute in the bulk solution and the formation of the external boundary film. The adsorption of lead ion on SCNP was done by two methods;

Table 1. Parameter values and regression coefficients for different kinetic models at 25 °C.

[Pb(II)] in ppm	Pseudo-first order models		Pseudo-second order models		Intra-particle diffusion models		
	$K_{I \pm 0.002}$ (h^{-1})	R^2	$K_{II \pm 0.002}$ ($g.mg^{-1}.h^{-1}$)	R^2	$K_{i \pm 0.01}$ ($mg.g^{-1}.h^{1/2}$)	I ($mg.g^{-1}$)	R^2
100	0.398	0.9583	0.597	0.9873	39.31	-21.38	0.9602
200	0.552	0.9799	0.671	0.9889	72.25	-59.47	0.9803
300	0.559	0.9565	0.110	0.9958	81.36	-74.74	0.9217
400	0.624	0.9226	0.134	0.9933	98.32	-75.80	0.9522
500	0.664	0.9328	0.257	0.9970	142.48	-105.30	0.9533
600	0.771	0.9267	0.277	0.9953	165.20	-167.35	0.9459
Average	0.595	0.9461	0.341	0.9930	99.82	-84.01	0.9520

a) The standing method using the water bath (0 rpm).
b) The shaking method using the shaker incubator at different speeds 50, 100 and 160 rpm for a contact of time 240 min and temperature of 25 °C.

Figure 5 shows the variation of q_e versus C_e. Shaking was found to have higher capacity q than standing. As the speed increases, the suspension becomes homogeneous due to the rapid agitation. The film boundary layer surrounding particles is reduced thus increasing the external film transfer coefficient, and hence the adsorption capacity. This result is surprising since the agitation speed can change the kinetics, not the equilibrium capacity. McKay [35] reported that the rate of heavy metal removal was influenced by the degree of agitation and the uptake increased with stirring rate. The degree of agitation reduced the boundary layer resistance and increased the mobility of the system. An agitation speed of 160 rpm was chosen for further experiments, Figure 5.

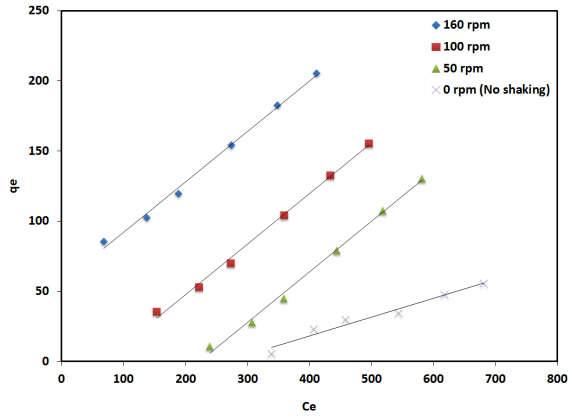

Figure 5. Comparison of adsorption of SCNP onto Pb(II) at 25 °C by: a) Standing method (0 rpm) and b) Shaking method (50,100 and 160 rpm).

4.3. Effect of contact time on the uptake of lead

The equilibrium time was measured from 1 to 168 hours. By plotting the percentage uptake of Pb(II) against contact time. It was found that the removal rate of Pb(II) was very fast for the first 3 hours, and reached maximum after 6 hours.

4.4. Effect of temperature

The rise in temperature increased the values of q_e and K_I. Therefore, the enhancement of adsorption capacity at higher temperatures may be attributed to the enlargement of pore size and/or activation of adsorbent surface. Plots of $1/q$ vs. $1/C$ for the adsorption of SCNP by Pb(II) at different temperatures (25, 30, 35 and 40 °C) indicates that the capacity "q" increases with increasing temperature.

4.5. Adsorption kinetics

The experimental data were fitted to both pseudo-first-order and pseudo-second-order models respectively, and the parameters obtained for are presented in Table 1. The good fitting of the models was expressed by the linear regression coefficients of determination (R^2); a relatively high R^2 value indicates that the model successfully describes the kinetics of Pb(II) sorption by SCNP.

Plot of log (q_e - q_t) versus t gives a straight line for pseudo-first-order kinetics. It allows the computation of the adsorption rate constant K_I where the slope is equivalent to -K_I/2.303 and the intercept is equivalent to log q_e. Adsorption rate constant K_I is shown in Table 1 as well as regression coefficient R^2. Figure 6 shows that for a Pseudo-second-order sorption kinetics the plots of t/q_t versus t gives a straight line with slope of $1/q_e$ and intercept $1/K_{II}q_e^2$. Using the value of q_e calculated from the slope, the value of K_{II} is determined from the intercept. The calculated value of K_{II} and its corresponding regression coefficient (R^2) values are presented in Table 1.

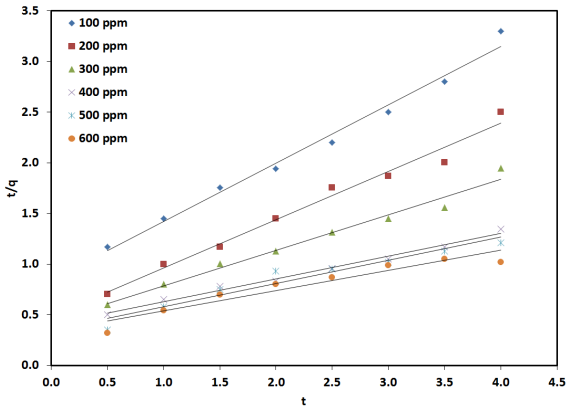

Figure 6. Pseudo-second-order sorption kinetics of SCNP at different Pb(II) concentrations (Adsorbent dose=0.05 g, T =25 °C).

According to R^2 values (Table 1) it can be concluded that the sorption process follows the pseudo-second-order adsorption rate: "If the intercept value does not equal log (q_e), the reaction is not likely to obey a pseudo-first-order kinetic model" [36]. The values of R^2 indicated that the intra-particle-diffusion kinetic model produced good results (Table 1) at all concentrations, R^2 values for this kinetic model were found to be high (between 0.9217 and 0.9803). The adsorption system obeys the intra-particle-diffusion kinetic model for the entire sorption period. Adsorption is a multi-step process involving transport of the solute molecules from the aqueous phase to the surface of the solid particles followed by diffusion of the solute molecules into the pore interiors. The fitness of intra-particle-diffusion kinetic model indicates that the mechanism for Pb(II) removal by adsorption on silica-carbon nanoparticles material is taking place through four steps:

a) Migration of Pb(II) molecules from the bulk solution to the surface of the adsorbent through bulk diffusion,
b) Diffusion of Pb(II) molecules through the boundary layer to the surface of the adsorbent via film diffusion,
c) The transport of the Pb(II) molecules from the surface to the interior pores of the particle occurs through intra-particle diffusion or pore diffusion mechanism, and

Table 2. Optimal parameters values for the Linear and non linear isotherm models at T = 25 - 40 °C.

Model, parameters and error	T = 25 °C		T = 30 °C		T = 35 °C		T = 40 °C	
	Non Linear	Linear	Non Linear	Linear	Non Linear	Linear	Non Linear	Linear
Langmuir								
Q^0	384.63	384.62	301.63	294.12	266.77	270.27	246.66	263.16
K_L	0.0018	0.0018	0.0038	0.0040	0.0072	0.0072	0.0150	0.0120
R^2	0.9984	0.9889	0.9924	0.9859	0.9859	0.9859	0.9799	0.9795
Freundlich								
n_F	1.43	1.36	1.92	1.78	2.65	2.33	3.20	3.10
K_F	2.13	2.02	6.95	6.46	15.99	15.58	33.94	31.86
R^2	0.9941	0.9928	0.9981	0.9977	0.9996	0.9966	0.9911	0.9876
Temkin								
B_T	75.31	74.12	67.90	66.61	61.45	58.53	53.14	49.49
K_T	0.040	0.022	0.041	0.037	0.081	0.072	0.260	0.190
R^2	0.9910	0.9880	0.9840	0.9820	0.9810	0.9720	0.9731	0.9539
Elovich								
Q	0.0043	0.0036	0.0071	0.0065	0.0100	0.0094	0.0140	0.0130
K_E	206.45	204.29	234.25	229.17	356.34	353.20	405.35	402.00
R^2	0.9721	0.9652	0.9890	0.9798	0.9631	0.9588	0.9465	0.9299

d) The adsorption of Pb(II) at an active site on the surface of material by chemical reaction via ion-exchange, complexation and/or chelation.

In a batch system with rapid stirring, there is a possibility that the transport of adsorbate from solution into the pores (bulk) of the adsorbent is the rate controlling step. This possibility was tested in terms of a graphical relationship between the amount of Pb(II) adsorbed and the square root of time. q_t was plotted against $t^{1/2}$ for different initial Pb(II) concentrations (Table 1). It was found that for all the four concentrations, the plots are linear with slope (K_i) and intercept (I), linearity is reduced with increasing concentration. The plots do not pass through the origin. The values of K_i and I are summarized in Table 1 along with the regression constant (R^2) for different initial Pb(II) concentrations.

The values of regression coefficient for all the six concentrations of SCNP confirm that, the sorption kinetics can be best described by pseudo-second-order adsorption model, Table 1.

4.6. Adsorption isotherm

The distribution of Pb(II) between the adsorbent and the solution at equilibrium has been expressed using various equations. Two widely used forms are the Langmuir and the Freundlich isotherms. The sorption data were analyzed according to the linear and non-linear form of Langmuir isotherm Equation (7) and (8). The Langmuir constants are reported in Table 2. The isotherm was found to be linear over the entire concentration range studied with a good linear correlation coefficient, showing that data correctly fit the Langmuir relation. The monolayer saturation capacity, Q_{max} was found to 384.62 mg/g. The fact that Langmuir isotherm fits the experimental data very well confirms the monolayer coverage of Pb(II) onto particles and also the homogenous distribution of active sites on the material, since the Langmuir equation assumes that the surface is homogenous.

Langmuir-type adsorption process can be classified by a dimensionless constant separation factor (R_L), given by Equation (9). It was observed that the value of R_L is closer to 1.00 confirms a favorable linear uptake.

Examination of the linear Freundlich isotherm plot Figure 7, indicated that the Freundlich model yielded a better fit than the Langmuir model, and that sorption occurs on heterogeneous surfaces. Table 2 shows the Freundlich constants, K_F and n_F, and R^2 for both linear and nonlinear forms. The value of R^2 was higher than the corresponding Langmuir isotherm R^2 values. The value of Freundlich exponent n_F is in the range 1-3 (Table 2), which indicates favorable adsorption.

In the case of Temkin model and Elovich model (Table 2) the deduced constants for linear and nonlinear models show greater difference, with lower R^2 values. This implies that these two models are not applicable to this study, and the sorption mechanism does not involve a multilayer adsorption and that the adsorption sites do not increase exponentially. Overall, the results revealed that regression coefficient values (R^2) were found to be higher in all nonlinear isotherm models than those obtained using linear model.

In general, determination of the best fitting isotherm model is based on the use of the 10 error functions described in Table 3, [24,37] by calculating the error deviation between experimental and predicted equilibrium adsorption data, for nonlinear analysis. From the values of non '*r*' error functions (smallest one)(ARED, MPSED, and HYBRID) and "*r*" containing error functions (highest one)(R^2, *r*, and r^2) in the overall results of the considered four models one can conclude that Freundlich model represents the best fitting curve using nonlinear expression.

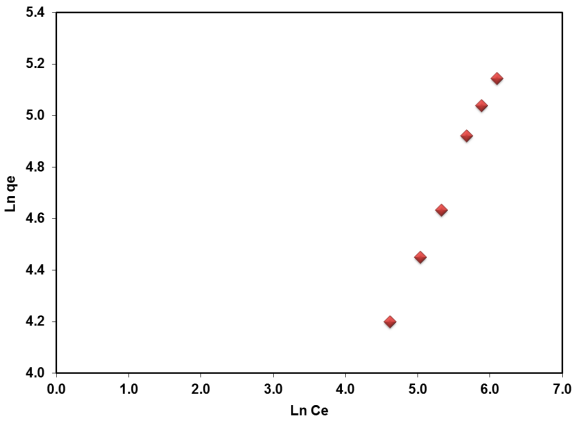

Figure 7. Freundlich isotherm plots for the adsorption of SCNP by Pb(II) at 25 °C.

4.7. Thermodynamics parameters

The adsorption equilibrium constant K_d which is equal to C_s/C_e has been calculated. Using the Van't Hoff Equation Ln K_d versus 1/T was plotted, Figure 8. The enthalpy $\Delta H°$ and entropy, $\Delta S°$ values were calculated from the slope and intercept, respectively. The results are shown in Table 4. The values of $\Delta G°$ being equal to $\Delta H° - T\Delta S°$ were also calculated.

In the present study, $\Delta H°$ was found to be negative in all concentrations of lead indicating that the interaction between lead and SCNP is exothermic and that the uptake involves physical adsorption.

Table 3. Isotherm error values with the considered nonlinear models, at different temperatures T (°C).

Model, parameters and error	R^2	$F(x)$	ARED	MPSED	HYBRID	χ^2	SSE	RMSE	r	r^2
Langmuir										
T = 25 °C	0.9991	$6.35x10^{-8}$	0.0141765	1.993680	2.1264890	$1.37x10^{-5}$	$1.27x10^{-7}$	$2.11x10^{-8}$	0.99953	0.999059
T = 30 °C	0.9991	$3.07 x10^{-7}$	0.0346021	4.865749	5.1903231	$7.67x10^{-5}$	$6.14x10^{-7}$	$1.02x10^{-7}$	0.994991	0.990007
T = 35 °C	0.9604	$6.42x10^{-7}$	0.0601279	8.338383	9.0191889	0.000188	$1.28x10^{-6}$	$2.14x10^{-7}$	0.979979	0.960358
T = 40 °C	0.9067	$8.94x10^{-7}$	0.0842390	11.53083	12.635850	0.0003	$1.79x10^{-6}$	$2.99x10^{-7}$	0.95219	0.906665
Freundlich										
T = 25 °C	0.9928	0.003599	0.006466	0.920017	0.969893	0.001549	0.007198	0.0012	0.996408	0.99283
T = 30 °C	0.9977	0.00082	0.00298	0.404578	0.447024	0.000328	0.00164	0.00027	0.998847	0.997695
T = 35 °C	0.9966	0.000906	0.003036	0.434191	0.455333	0.000368	0.001812	0.00030	0.998304	0.996611
T = 40 °C	0.9876	0.002588	0.005349	0.72495	0.802307	0.001039	0.005176	0.00086	0.993791	0.98762
Temkin										
T = 25 °C	0.988	61.36155	0.044368	7.139272	6.655227	1.504854	122.7231	20.4538	0.993974	0.987985
T = 30 °C	0.982	91.95516	0.044325	6.91669	6.648681	1.805941	183.9103	30.6517	0.990956	0.981995
T = 35 °C	0.972	142.9453	0.047267	7.133717	7.090033	2.335133	285.8906	47.6484	0.985906	0.97201
T = 40 °C	0.9539	235.224	0.053252	7.775615	7.987807	3.266603	470.4479	78.4079	0.976699	0.953942
Elovich										
T = 25 °C	0.9652	68.92243	-5.9388	745.4096	-890.82	-23.1482	137.8449	22.9741	0.982467	0.965242
T = 30 °C	0.9798	98.38275	-	-	-	-30.4281	196.7655	32.7942	0.989862	0.979827
T = 35 °C	0.9618	136.8868	1.764799	4114.166	264.7199	-38.5463	273.7735	45.6289	0.980708	0.961788
T = 40 °C	0.9602	181.119	7.232771	5038.571	1084.916	-46.5569	362.238	60.373	0.979875	0.960154

Table 4. Thermodynamic parameters of adsorption of lead onto SCNP at different temperatures.

Concentration of lead (mg/L)	K_D ± 0.005	$\Delta H°$ ± 0.05 (kJ/mol)	$\Delta S°$ ± 0.1 (J/mol.K)	$\Delta G°$ ± 0.05 (kJ/mol)			
				298 K	303 K	308 K	313 K
100	1.033	-82.76	273.27	-81.50	-82.88	-84.25	-85.62
200	1.018	-45.20	146.77	-43.78	-44.52	-45.25	-45.98
300	1.014	-35.80	114.39	-34.12	-34.70	-35.27	-35.84
400	1.010	-26.49	82.63	-24.65	-25.06	-25.48	-25.89
Average	1.019	-47.56	154.26	-46.02	-46.79	-47.56	-48.33

The positive value of ΔS° suggested an increase in randomness at the solid-solution interface during the adsorption. At all temperatures the negative values of ΔG shows that the adsorption was spontaneous.

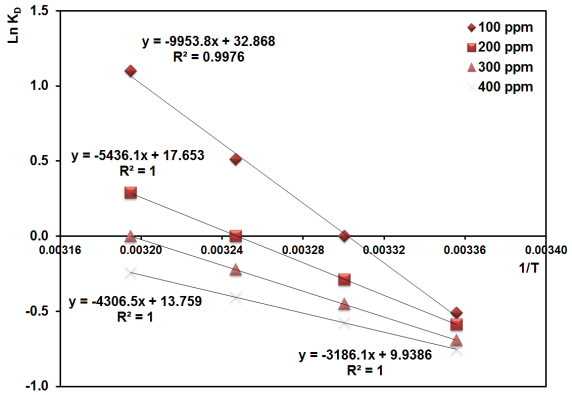

Figure 8. Plot of Ln KD versus 1/T for the adsorption of lead onto SCNP at different metals concentrations.

4.7.1. Thermodynamics of activation

The values of activation thermodynamic parameters E_a, $\Delta H^{\neq}$, $\Delta S^{\neq}$ and $\Delta G^{\neq}$ values for Pb(II) removal by SCNP are reported in Table 5 using the Van't Hoff Equation and plotting Ln K_{II} versus 1/T, Figure 9; or Using Eyring equation and plotting Ln K_{II}/T versus 1/T, Figure 10, where K_{II} is the rate constant for pseudo-second order kinetic. The enthalpy and entropy values were calculated from the slope and intercept, respectively.

4.8. Column studies

4.8.1. Column adsorption studies

Column studies were conducted using a Pyrex glass column (20 cm length x 1 cm diameter) down flow technique (Flow rate 2 ml/min), 0.5 g of SCNP was transferred into the glass column. Glass was kept at the bottom of the column to avoid the loss of adsorbent with the liquid flow. The Pb(II) solution of 500 mg/L initial concentration was fed into the column at a flow rate of 2 mL/min and definite volumes of the effluent were collected. The amount of lead retained by the adsorbent was then determined.

A breakthrough graph was plotted for C/C_0 versus volume V (mL) of solution eluted. The maximum volume that can be treated was found to be about 200 mL, Figure 11. The percentage of Pb(II) removal was also plotted against the volume V (mL) for the three different cycles. It was found that after cycle number 3 the column efficiency is greatly reduced. The amount of Pb(II) adsorbed q_t (mg/g) as a function of V (mL) of Pb(II) added was calculated for three different consecutive cycles. The total adsorption capacity of SCNP for lead(II) was found to be 50 mg/g for the first cycle and 90 mg/g for overall three consecutive cycles.

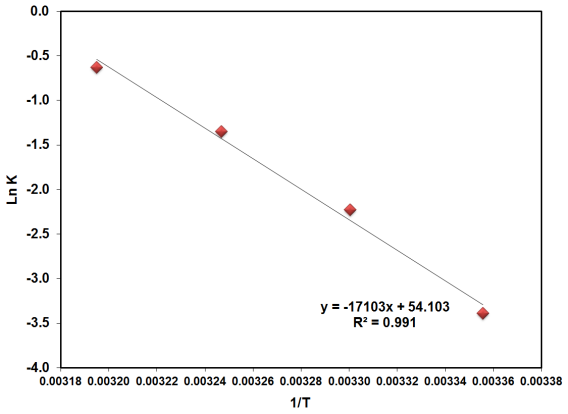

Figure 9. Van't Hoff Plot of Ln K_{II} versus 1/T.

Table 5. Activated thermodynamic parameters of adsorption of lead onto SCNP at different temperatures. (Pollutant concentration: 300 ppm, mass of adsorbent: 0.05, Volume of metal solution: 50 mL).

T (K)	K_{II} ±0.002 ($g.mg^{-1}.h^{-1}$)	Ea ± 0.05 (KJ/mol)	$\Delta H^{\#}$ ± 0.05 (KJ/mol)	$\Delta H^{\#}$ ± 0.05 (KJ/mol)	$\Delta S^{\#}$ ± 0.1 (KJ/mol)	$\Delta G^{\#}$ ± 0.1 (KJ/mol)
			Arrhenius	Eyring		
298	0.034	142.13	139.65	139591.4	-20.58	81.10
303	0.108	142.13	139.61	139591.4	-20.92	80.12
308	0.260	142.13	139.57	139591.4	-21.27	79.13
313	0.531	142.13	139.53	139591.4	-21.61	78.15

Table 6. Linear and nonlinear approach of Thomas, Yoon-Nelson and Yan's model.

Model	Linear approach			Non-Linear approach		
Thomas	K_{th} (mL.(mg.min)$^{-1}$)	q_T (mg.g^{-1})	R^2	K_{th} (mL.(mg.min)$^{-1}$)	q_T (mg.g^{-1})	R^2
	0.0646	118.56	0.665	0.067	119.62	0.701
Yoon-Nelson	k_{YN} (min^{-1})	τ_{YN} (min)	R^2	k_{YN} (min^{-1})	τ_{YN} (min)	R^2
	0.0320	59.27	0.665	0.033	59.88	0.735
Yan's	k_Y (mL.mg^{-1}.min^{-1})	q_Y (mg.g^{-1})	R^2	k_Y (mL.mg^{-1}.min^{-1})	q_Y (mg.g^{-1})	R^2
	0.00724	130.66	0.937	0.0074	134.90	0.957

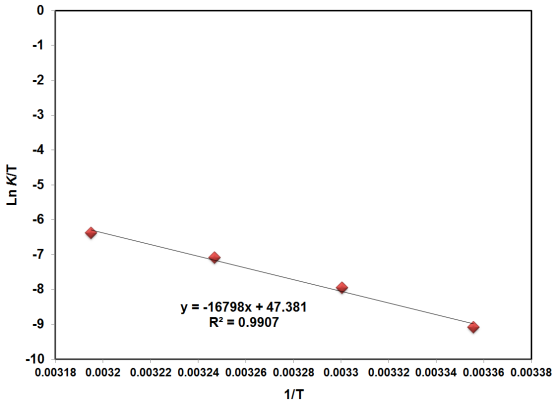

Figure 10. Eyring plot of Ln K_{II}/T versus 1/T.

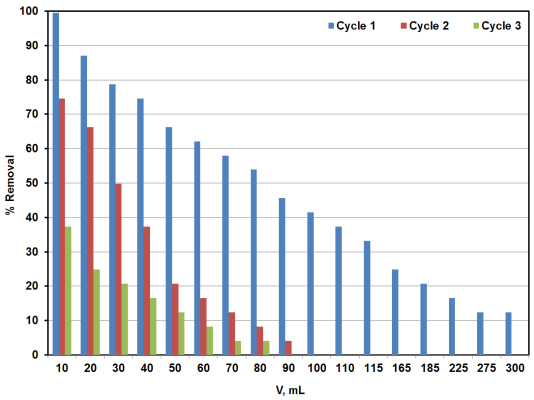

Figure 11. Variation of % Pb(II) Removal as a function of volume V (mL) of Pb(II) (300 ppm) added for sorption of Pb(II) onto SCNP column.

4.8.2. Column desorption studies

The SCNP loaded with Pb(II) ions was regenerated with 0.1 M HCl (Flow rate 2 mL/min) after exhaustion. It was found that each column regeneration requires washing with 400 mL of HCl (0.1 M).

4.8.3. Column models

Thomas, Yoon nelson and Yan models were applied according to the equations 16, 17 and 18; the results are presented in Table 6, where the maximum capacity and the rate constant for each model are tabulated, Table 6. Application of Yoon Nelson model indicated that τ the half life of adsorbate breakthrough is equal to 59.88 min (non linear approach). A comparison of the three correlation coefficients (R^2) indicates that Yan et al. model fits best the experimental breakthrough curves, with R^2 equal to 0.937, with q_y =130.66 mg/g (0.63 mmol/g), Figure 12.

Q_{max} was also calculated using the integration method Equation (19) and the plot of Concentration of lead (mg/L) adsorbed vs. time (min). Q_{max} was found to be equal to 102 mg/g (0.49 mmol/g).

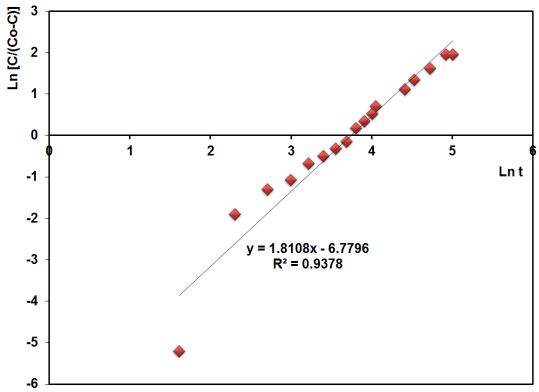

Figure 12. Linear plot of the Yan *et al.* model for the removal of lead by SCNP.

5. Conclusion

Despite the promising achievements and plausible prospects of carbon nanostructures, problems are associated with their production in large scales, without any defects, and in short time. Therefore their sonochemical production is one of the newly promising methods under ambient conditions. The equilibrium data were well fitted in terms of the Freundlich and Langmuir adsorption isotherm models. The maximum adsorption capacity was relatively higher than other adsorbent material (Table 7) [38-42] and found to be 385 mg/g (1.86 mmol/g). The thermodynamic parameters have been obtained, and showed that the sorption process of SCNP onto lead was spontaneous and exothermic.

Table 7. Comparison of maximum adsorption capacities of various materials for Pb(II) removal.

Adsorbent	q max (mg/g)	Reference
Activated carbon 13 F-400	30.11	[38]
Acidified MWCNTs	49.71	[39]
Pine wood char	4.13	[40]
Native bentonite	19.19	[41]
Cicer arientinum biomass	27.79	[42]
Silica-Carbon nanoparticles	384.63	This study

The kinetic adsorption processes were described by a pseudo-second order model. Column studies also proved the suitability of SCNP and its potential to withstand different conditions and be regenerated without losing its metal sorption capacity. In general, the cheaply prepared SCNP can be used in wastewater treatments as adsorbent for lead removal.

References

[1]. Dresselhaus, M. S.; Dresselhaus, G.; Eklund, P. C. Science of Fullerenes and Carbon Nanotubes; Academic Press: San Diego, CA, 1996.
[2]. Endo, M.; Hayashi, T.; Ahm, K. Y. *Pure Appl. Chem.* **2006**, *78*, 1703-1713.
[3]. Huang, H.; Kajiura, H.; Tsutsui, S.; Hirano, Y.; Miyakoshi, M.; Yamada, A.; Ata, M. *Chem. Phys. Lett.* **2001**, *343(1-2)*, 7-14.
[4]. Hafner, J. H.; Bronikowski, M. J.; Azamian, B. R.; NikoLaevl, P.; Rinzler, A. G.; Colbert, D. T.; Smith, K. A.; Smalley, R. E. *Chem. Phys. Lett.* **1998**, *296(1-2)*, 195-202.
[5]. Che, G.; Lakshmi, B. B.; Martin, C. R.; Fisher, E. R.; Ruoff, R. S. *Chem. Mater.* **1998**, *10(1)*, 260-267.
[6]. Laplaze, D.; Bernier, P.; Maser, W. K.; Flamant, G.; Guillard, T.; Loiseau, A. *Carbon* **1998**, *36(5-6)*, 685-688.
[7]. Suslick, K. S. *MRS Bull.* **1995**, *20*, 29-33.
[8]. Jeong, S. H.; Ko, J. H.; Park, J. B.; Park, W. *J. Am. Chem. Soc.* **2004**, *126(49)*, 15982-15983.
[9]. Stafiej, A.; Pyrzynska, K. *Sep. Purif. Technol.* **2008**, *58*, 49-52.
[10]. Hsieh, S. H.; Horng, J. J. *J. Univ. Sci. Technol. Beijing* **2007**, *14(1)*, 77-84.
[11]. Li, Y. H.; Wang, S.; Wei, J.; Zhang, X.; Xu, C.; Luan, Z.; Wu, D.; Wei, B. *Chem. Phys. Lett.* **2002**, *357*, 263-266.
[12]. Li, Y. H.; Wang, S.; Luan, Z.; Ding, J.; Xu, C.; Wu, D. *Carbon* **2003**, *41*, 1057-1062.
[13]. Deng, S.; Bai, R. *Water Res.* **2004**, *38*, 2424-2432.
[14]. Andrews, R.; Jacques, D.; Rao, A. M.; Derbyshire, F.; Qian, D.; Fan, X.; Dickey, E. C. Chen, J. *Chem. Phys. Lett.* **1999**, *303*, 467-474.
[15]. Volesky, B. Sorption and Biosorption. B. V. Sorbex, Inc. Montreal, Canada, 2003.
[16]. Hao, O. J.; Kim, H.; Chiang, P. C. *Crit. Rev. Environ. Sci. Technol.* **2000**, *30*, 449-505.
[17]. Lagergren S. *Kungliga Svenska Vetenskapsakademiens, Handlingar* **1898**, *24(4)*, 1-39.
[18]. Ho, Y. S. *Scientometrics* **2004**, *59*, 171-177.
[19]. Purkait, M. K.; Gusain, D. S.; DasGupta, S.; De, S. *Separ. Sci. Technol.* **2004**, *39(10)*, 2419-2440.
[20]. Ho, Y. S.; McKay, G. *Trans. IChemE.* **1998**, *76*, 332-340.
[21]. Ho, Y. S; Wase, D. A. J.; Forster, C. F. *Environ. Technol.* **1996**, *17*, 71-77.
[22]. Weber, W. J.; Morris, J. C. *J. Sanit. Eng. Div. Proceed. Am. Soc. Civ. Eng*. **1963**, *89*, 31-39.
[23]. Ho, Y. S. *Water Res.* **2003**, *37*, 2323-2330.
[24]. Hammud, H.; Lina, F. L.; Holail, H.; Mostafa, E. S. M. E. *Int. J. Chem.* **2011**, *3(4)*, 147-163.
[25]. Langmuir, I. *J. Am. Chem. Soc.* **1918**, *40*, 1361-1403.
[26]. Hall, K. R.; Eagleton, L. C.; Acrivos, A.; Vermeulen, T. *Ind. Eng. Chem.* **1966**, *5*, 212-219.
[27]. McKay, G. *J. Chem. Technol. Biotechnol.* **1982**, *32*, 759-772.
[28]. Weber, T. W.; Chakravorti, R. K. *J. Am. Inst. Chem. Eng*. **1974**, *20*, 228-238.
[29]. Freundlich, H. M. F. *Z. Phys. Chem.* **1906**, *57*, 385-470.
[30]. Ho, Y. S.; Porter, J. F.; McKay, G. *Water Air Soil Pollut.* **2002**, *141*, 1-4.
[31]. Malkoc, E.; Nuhoglu, Y. *Chem. Eng. Sci.* **2006**, *61*, 4363-4372.
[32]. Sivakumar, P.; Palanisamy, P. N. *Indian J. Chem. Tech.* **2009**, *16*, 301-303.
[33]. Yoon, Y. H.; Nelson, J. H. *Am. Ind. Hyg. Assoc. J.* **1984**, *45*, 509-516.
[34]. Yan, G. Y.; Viraraghavan, T.; Chen, M. *Adsorp. Sci. Tech*. **2001**, *19*, 25-43.
[35]. McKay, G. *J. Chem. Technol. Biotechnol.* **1982**, *32*, 759-772.
[36]. Ho, Y. S.; McKay, G. *Can. J. Chem. Eng.* **1998**, *76*, 822-826.
[37]. Ncibi, M. C. *J. Hazard. Mater.* **2008**, *153*, 207-212.
[38]. Kim, K. S.; Choi, H. C. *Water Sci. Technol.* **1998**, *38(4-5)*, 95-101.
[39]. Wang, H. J.; Zhou, A. L.; Peng, F.; Yu, H.; Chen, L. F. *Mater. Sci. Eng. A* **2007**, *466*, 201-206.
[40]. Mohan, D.; Pittman, J. C. U.; Bricka, M.; Smith, F.; Yancey, B.; Mohammad, J.; Steele, P. H.; Alexandre-Franco, M. F.; Gomez-Serrano, V.; Gong, H. *J. Colloid Interface Sci.* **2007**, *310*, 57-73.
[41]. Kul, A. R.; Koyuncu, H. *J. Hazard. Mater.* **2010**, *179*, 332-339.
[42]. Nadeem, R.; Nasir, M. H.; Hanif, M. S. *Chem. Eng. J.* **2009**, *150*, 40-48.